NUMERICAL SOLUTION OF THE PHASE AVERAGE NAVIER-STOKES EQUATION USING THE FINITE ELEMENT METHOD

J. van der Westhuizen* J. Prieur du Plessis†

(First version August 1995; Final version August 1995)

Abstract

Recent solutions proposed for the surface integral term contained in the phase average form of the Navier-Stokes equation has transformed the equation into a practical tool for the numerical analysis of macroscopic flow through porous media. In this paper the form of these equations, governing the transport of momentum through porous media for low Reynolds number laminar flow of incompressible fluids, is cast into a set of algebraic equations using the Ritz finite element method. The continuity requirement is treated as a constraint condition and is incorporated into the algebraic equations through the penalty function method. The final set of algebraic equations is coded into a finite element software program in order to demonstrate the proposed numerical solution method. Numerical solutions included illustrate the transition from Navier-Stokes to phase average Navier-Stokes to Darcy-type controlled flow in porous media as the shear flow resistance of the porous medium is increased relative to the viscosity of the traversing fluid. In addition to this, the versatility of the proposed numerical method is demonstrated with the solution of a flow front problem for the case where a fluid penetrates into a 'dry' porous domain.

Nomenclature

$\mathcal{B}$	functional
$\overline{b}_i$	volumetric intrinsic phase average of body force per unit volume
$\mathbf{F}$	column matrix of nodal forces
F_{ij}	microscopic flow resistance
$\mathcal{F}$	functional
$\mathcal{F}_p$	modified functional
G	constraint function
$\mathbf{K}$	global coefficient matrix
K_{ij}	hydrodynamic permeability
$\mathcal{L}$	functional
m	number of modes per finite element
$\hat{n}_i$	Cartesian unit base vectors
$\overline{p}$	volumetric intrinsic phase av. of fluid pressure
$\mathbf{q}$	column matrix of nodal specific discharge degrees of freedom
q_i	specific discharge
$q_{i\beta}$	specific discharge degrees of freedom
t_i	natural boundary condition on finite element
ω	weight or test function
x_i	coordinate
$\in$	porosity
μ	fluid dynamic viscosity
γ	penalty parameter
Γ	finite element boundary surface
Ψ_β	finite element interpolation functions
Ω	finite element domain

Notes:

- Cartesian tensor notation is indicated with lower case (non-italic) Arabic subscripts.
- Bold upper case Arabic letters denote matrices and bold lower case Arabic letters denote column matrices.

Introduction

The solution of transport problems in porous media presents a challenging research field with potential benefit in a diverse number of engineering areas such as ground water seepage, cellular bone behaviour, crushable foam structures, air pollution of forest areas, and composite material processes.

The general approach to obtaining numerical solutions in this field is based on using the tensorized Darcy[1]

*Senior Lecturer (Member), Department of Mechanical Engineering, University of Stellenbosch, Stellenbosch, 7600 South Africa

†Associate Professor, Department of Applied Mathematics

equation (1), together with the continuity equation (2) as governing equations. A recent application of this methodology can be found in the work of Bruschke & Advani.[2]

$$q_i = -\frac{1}{\mu} K_{ij} P_{,j} \tag{1}$$

$$q_{i,i} = 0 \tag{2}$$

Equation (1) has the disadvantage that macroscopic phenomena such as the no-slip velocity boundary conditions are implicitly ignored. This may be quite acceptable for cases where the permeability of the porous medium is very low compared to the viscosity of the traversing fluid, but can certainly lead to erroneous results in other situations.

A momentum transport equation governing flow in porous media that includes macroscopic flow effects has however been available for some time. The equation is largely the result of applying an averaging theorem developed by Slattery[3] and Whitaker[4] rigorously to the standard Navier-Stokes equation. The reader is referred to Bear & Bachmat,[5] and Du Plessis & Masliyah[6] for an overview and derivation of this equation, which is also referred to as the phase average form of the Navier-Stokes equation.

Until recently the phase-average form of the Navier-Stokes equation was not readily suitable for numerical analysis since it contains an 'unfriendly' surface integral term that captures the micro-scale fluid/solid interaction. The numerical solution of this integral term is not practical since the integration has to be performed over the micro-scale surface area of the porous domain structure. The only other (but unsatisfactory) alternative was to approximate the surface integral term with empirical formulae. Fortunately this shortcoming was overcome by Du Plessis & Masliyah[6] who proposed a solution methodology to closure of the surface integral term that culminated in the form of the phase average Navier-Stokes equation shown in equation (3) and incorporates the shear flow resistance factor F. Van der Westhuizen & Du Plessis[7] extended the shear flow resistance concept to orthotropic media and set up the tensorial form for the surface integral term contained in equation (3). For low Reynolds number incompressible steady state laminar flow an alternative and more inclusive equilibrium equation is therefore established as

$$0 = \bar{b}_i - \in \bar{p}_{,i} + \left[\mu\left(q_{i,j} + q_{j,i}\right)\right]_{,j} - \mu F_{ij} q_j \tag{3}$$

In the equation above the terms on the right hand side represent, respectively, the body forces, the pressure gradient, the viscous shear forces and the shear resistance of the porous domain to fluid flow.

This paper sets up the finite element algebraic equations equivalent to the governing differential equations (2) and (3), describes a software program that was developed to solve these algebraic equations numerically and illustrates typical results. The general finite element methodology followed here is formulated in detail in several text books of which Reddy[8] is recommended.

Theoretical development

Weak form of the governing equations

The integral form of equation (3) is constructed by multiplying the equation with a test or weight function, ω, and integrating this product over the domain of a general finite element as follows:

$$0 = \int_{\Omega} \omega \left[-\bar{b}_i + \in \bar{p}_{,i} - \left[\mu\left(q_{i,j} + q_{j,i}\right)\right]_{,j} + \mu F_{ij} q_j\right] d\Omega \tag{4}$$

In this way the governing equation will be satisfied in an average or integral sense over each finite element domain.

Equation (4) is now further manipulated in order to achieve the same continuity requirement for the weight function as for the unknown fields and to isolate the natural boundary conditions explicitly as part of the formulation. The first step is to apply the product rule of differentiation as follows:

$$\begin{aligned} 0 = \int_{\Omega} \{ & -\omega \bar{b}_i + \in (\omega \bar{p})_{,i} - \in \omega_{,i} \bar{p} \\ & - \left(\omega \mu \left(q_{i,j} + q_{j,i}\right)\right)_{,j} \\ & + \omega_{,j} \mu \left(q_{i,j} + q_{j,i}\right) \\ & + \omega \mu F_{ij} q_j \} d\Omega \end{aligned} \tag{5}$$

The second step is to apply the gradient theorem (also known as Gauss' theorem) to the second and fourth terms of the integrand of equation (5), and assume that the porosity $\in$ can be taken as constant throughout each finite element, so that

$$\begin{aligned} 0 = \int_{\Omega} \{ & -\omega \bar{b}_i - \in \omega_{,i} \bar{p} + \omega_{,j} \mu \left(q_{i,j} + q_{j,i}\right) \\ & + \omega \mu F_{ij} q_j \} d\Omega - \oint \omega t_i d\Gamma. \end{aligned} \tag{6}$$

In the equation above the natural boundary condition, t_i, is given by

$$t_i = - \in \bar{p} \hat{n}_i + \mu \left(q_{i,j} + q_{j,i}\right) \hat{n}_j. \tag{7}$$

It is convenient and physically informative to express equations (6) and (7) in component form at this point. For the 1-direction the result is

$$0 = \int_{\Omega} \{-\omega \bar{b}_1 - \in \frac{\partial \omega}{\partial x_1}\overline{p} + \frac{\partial \omega}{\partial x_1}\left[\mu\left(\frac{\partial q_1}{\partial x_1} + \frac{\partial q_1}{\partial x_1}\right)\right] + \frac{\partial \omega}{\partial x_2}\left[\mu\left(\frac{\partial q_1}{\partial x_2} + \frac{\partial q_2}{\partial x_1}\right)\right] + \frac{\partial \omega}{\partial x_3} \times \left[\mu\left(\frac{\partial q_1}{\partial x_3} + \frac{\partial q_3}{\partial x_1}\right)\right] + \omega\mu\left(F_{11}q_1 + F_{12}q_2 + F_{13}q_3\right)\}d\Omega - \oint_{\Gamma} \omega t_1 d\Gamma, \tag{8}$$

where

$$t_1 = - \in \overline{p}\hat{n}_1 + \mu\left(\frac{\partial q_1}{\partial x_1} + \frac{\partial q_1}{\partial x_1}\right)\hat{n}_1 + \mu\left(\frac{\partial q_1}{\partial x_2} + \frac{\partial q_2}{\partial x_1}\right)\hat{n}_2 + \mu\left(\frac{\partial q_1}{\partial x_3} + \frac{\partial q_3}{\partial x_1}\right)\hat{n}_3 \tag{9}$$

The weak form of the continuity equation (2) is constructed in the same way as that of the momentum equation (3), but since only the first derivatives of specific discharge are contained in this equation, the derivative is not transferred to the weight function. In component form the result is given by

$$0 = \int_{\Omega} \omega\left[\frac{\partial q_1}{\partial x_1} + \frac{\partial q_2}{\partial x_2} + \frac{\partial q_3}{\partial x_3}\right] d\Omega \tag{10}$$

The associated functional

Addition of the three component equations represented by the tensor equation (6), i.e. the weak form of the governing momentum equation, leads to a single equation that can be recast into two functionals as follows:

$$\mathcal{B}\left(\left(\omega_1, \omega_2, \omega_3\right), \left(q_1, q_2, q_3\right)\right) = \mathcal{L}\left(\omega_1, \omega_2, \omega_3\right) \tag{11}$$

In the equation above ω_1, ω_2 and ω_3, are the weight functions respectively associated with each of the specific discharge components q_1, q_2 and q_3, and $\mathcal{B}$ is a functional, or function of these functions, given by

$$\mathcal{B} = \int_{\Omega} \{2\mu\left(\frac{\partial \omega_1}{\partial x_1}\frac{\partial q_1}{\partial x_1} + \frac{\partial \omega_2}{\partial x_2}\frac{\partial q_2}{\partial x_2} + \frac{\partial \omega_3}{\partial x_3}\frac{\partial q_3}{\partial x_3}\right) + \mu\left(\frac{\partial \omega_1}{\partial x_2} + \frac{\partial \omega_2}{\partial x_1}\right)\left(\frac{\partial q_1}{\partial x_2} + \frac{\partial q_2}{\partial x_1}\right) + \mu\left(\frac{\partial \omega_1}{\partial x_3} + \frac{\partial \omega_3}{\partial x_1}\right)\left(\frac{\partial q_1}{\partial x_3} + \frac{\partial q_3}{\partial x_1}\right) + \mu\left(\frac{\partial \omega_2}{\partial x_3} + \frac{\partial \omega_3}{\partial x_2}\right)\left(\frac{\partial q_2}{\partial x_3} + \frac{\partial q_3}{\partial x_2}\right) + \mu\omega_i F_{ij} q_j - \in \overline{p}\frac{\partial \omega_i}{\partial x_i}\}d\Omega \tag{12}$$

The functional $\mathcal{L}$ is given by

$$\mathcal{L} = \int_{\Omega} \omega_i \bar{b}_i d\Omega + \oint_{\Gamma} \omega_i t_i d\Gamma \tag{13}$$

A solution for the specific discharge field that satisfies the linear momentum equation (3) will also satisfy equation (11). In this context, equation (11) must hold for any weight functions that satisfy the essential boundary conditions and is therefore the variational problem associated with the governing equation (3). The weight functions ω_1, ω_2 and ω_3 are equivalent to variations δq_1, δq_2 and δq_3 of the velocity field.

This variational equivalence allows a simplification of the expression for $\mathcal{B}$, since

$$\frac{\partial \omega_1}{\partial x_1} + \frac{\partial \omega_2}{\partial x_2} + \frac{\partial \omega_3}{\partial x_3} \equiv \frac{\partial}{\partial x_1}\left(\delta q_1\right) + \frac{\partial}{\partial x_2}\left(\delta q_2\right) + \frac{\partial}{\partial x_3}\left(\delta q_3\right) \tag{14}$$

which is zero from continuity and thus implies that the last term in the integral of equation (12) vanishes.

Since the functional $\mathcal{B}$ is symmetric and bilinear (note that the flow resistance tensor F_{ij} is symmetric) and the functional $\mathcal{L}$ is linear, a functional $\mathcal{F}$ can be constructed as follows for which the extreme value solution also satisfies the conservation of linear momentum stated by the governing equation (3):

$$\begin{aligned}\mathcal{F}\left(q_1, q_2, q_3\right) &= \tfrac{1}{2}\mathcal{B}\left(\left(q_1, q_2, q_3\right), \left(q_1, q_2, q_3\right)\right) - \mathcal{L}\left(q_1, q_2, q_3\right) \\ &= \int_{\Omega} \{\mu\left(\frac{\partial q_1}{\partial x_1}\frac{\partial q_1}{\partial x_1} + \frac{\partial q_2}{\partial x_2}\frac{\partial q_2}{\partial x_2} + \frac{\partial q_3}{\partial x_3}\frac{\partial q_3}{\partial x_3}\right) \\ &\quad + \frac{\mu}{2}\left(\frac{\partial_1 q_1}{\partial x_2} + \frac{\partial q_2}{\partial x_1}\right)^2 + \frac{\mu}{2}\left(\frac{\partial q_1}{\partial x_3} + \frac{\partial q_3}{\partial x_1}\right)^2 \\ &\quad + \frac{\mu}{2}\left(\frac{\partial q_2}{\partial x_3} + \frac{\partial q_3}{\partial x_2}\right)^2 + \frac{\mu}{2}q_i F_{ij} q_j + q_i \bar{b}_i\}d\Omega - \oint_{\Gamma} q_i t_i dl\end{aligned} \tag{15}$$

It is straightforward to confirm that the functional of equation (15) is constructed correctly by generating the necessary equations to form a minimum of the functional. This is achieved by consecutively taking the first variation in each component of the specific discharge and equating it to zero. For example, consider the variation

$$\delta_{q_i}\mathcal{F} = \int_{\Omega} \{2\mu\frac{\partial q_1}{\partial x_1}\frac{\partial \delta q_1}{\partial x_1} + \mu\left(\frac{\partial_1 q_1}{\partial x_2} + \frac{\partial q_2}{\partial x_1}\right)\frac{\partial \delta q_1}{\partial x_2} + \mu\left(\frac{\partial q_1}{\partial x_3} + \frac{\partial q_3}{\partial x_1}\right)\frac{\partial \delta q_1}{\partial x_3} + \mu F_{11} q_1 \delta q_1 + \frac{\mu F_{12} q_2}{2}\delta q_1 + \frac{\mu F_{13} q_3}{2}\delta q_1 + \frac{\mu F_{21} q_2}{2}\delta q_1 + \frac{\mu F_{31} q_3}{2}\delta q_1 - \bar{b}_1 \delta q_1\}d\Omega - \oint_{\Gamma} t_1 \delta q_1 d\Gamma \tag{16}$$

which is equivalent to equation (8), except for the pressure term that disappears as a consequence of continuity.

The problem of finding an approximate numerical solution to the governing equations (2) and (3) in a certain

domain can therefore be restated in two alternative ways:

- Subdivide the domain into suitable finite elements. Find a solution to the weak form of the governing equations (6) and (10) over each finite element. Assemble the finite elements in a proper manner, i.e. ensure sufficient continuity and equilibrium between elements to guarantee convergence and accuracy of the solution.
- Subdivide the domain into suitable finite elements. Find the extreme value solution of the functional $\mathcal{F}$ of equation (11) subject to the continuity constraint of equation (2) over each finite element. Assemble the finite elements in a proper manner.

The second approach will be used here.

Constraint formulation

The penalty function method will be used to reformulate the stated constrained problem into a set of equations incorporating the constraint condition through a penalty parameter, γ. This is done by modifying the functional $\mathcal{F}$ as follows:

$$\mathcal{F}_{\mathrm{p}} = \mathcal{F} + \frac{1}{2}\gamma G^2 \tag{17}$$

where the continuity equation forms the constraint function G, given by

$$G(q_1, q_2, q_3) = \frac{\partial q_1}{\partial x_1} + \frac{\partial q_2}{\partial x_2} + \frac{\partial q_3}{\partial x_3} \tag{18}$$

The extreme value of the modified functional may now be found through variational principles that call for solving the following three equations simultaneously:

$$\begin{aligned} 0 &= \delta_{q_1}\mathcal{F}_{\mathrm{p}} \\ &= \int_{\Omega}\{2\mu\frac{\partial\delta q_1}{\partial x_1}\frac{\partial q_1}{\partial x_1} + \mu\frac{\partial\delta q_1}{\partial x_2}\left(\frac{\partial q_1}{\partial x_2} + \frac{\partial q_2}{\partial x_1}\right) \\ &\quad +\mu\frac{\partial\delta q_1}{\partial x_3}\left(\frac{\partial q_1}{\partial x_3} + \frac{\partial q_3}{\partial x_1}\right) + \mu\delta q_1 \\ &\quad \times (F_{11}q_1 + F_{12}q_2 + F_{13}q_3)\}d\Omega \\ &\quad +\gamma\int_{\Omega}\frac{\partial\delta q_1}{\partial x_1}\left(\frac{\partial q_1}{\partial x_1} + \frac{\partial q_2}{\partial x_2} + \frac{\partial q_3}{\partial x_3}\right)d\Omega \\ &\quad -\int_{\Omega}\rho\delta q_1\bar{b}_1 d\Omega - \oint_{\Gamma}\delta q_1 t_1 d\Gamma \end{aligned} \tag{19}$$

$$\begin{aligned} 0 &= \delta_{q_2}\mathcal{F}_{\mathrm{p}} \\ &= \int_{\Omega}\{2\mu\frac{\partial\delta q_2}{\partial x_2}\frac{\partial q_2}{\partial x_2} + \mu\frac{\partial\delta q_2}{\partial x_1}\left(\frac{\partial q_1}{\partial x_2} + \frac{\partial q_2}{\partial x_1}\right) \\ &\quad +\mu\frac{\partial\delta q_2}{\partial x_3}\left(\frac{\partial q_2}{\partial x_3} + \frac{\partial q_3}{\partial x_2}\right) + \mu\delta q_2 \\ &\quad \times (F_{21}q_1 + F_{22}q_2 + F_{23}q_3)\}d\Omega \\ &\quad +\gamma\int_{\Omega}\frac{\partial\delta q_2}{\partial x_2}\left(\frac{\partial q_1}{\partial x_1} + \frac{\partial q_2}{\partial x_2} + \frac{\partial q_3}{\partial x_3}\right)d\Omega \\ &\quad -\int_{\Omega}\rho\delta q_2\bar{b}_2 d\Omega - \oint_{\Gamma}\delta q_2 t_2 d\Gamma \end{aligned} \tag{20}$$

and

$$\begin{aligned} 0 &= \delta_{q_3}\mathcal{F}_{\mathrm{p}} \\ &= \int_{\Omega}\{2\mu\frac{\partial\delta q_3}{\partial x_3}\frac{\partial q_3}{\partial x_3} + \mu\frac{\partial\delta q_3}{\partial x_1}\left(\frac{\partial q_1}{\partial x_3} + \frac{\partial q_3}{\partial x_1}\right) \\ &\quad +\mu\frac{\partial\delta q_3}{\partial x_2}\left(\frac{\partial q_2}{\partial x_3} + \frac{\partial q_3}{\partial x_2}\right) + \mu\delta q_3 \\ &\quad \times (F_{31}q_1 + F_{32}q_2 + F_{33}q_3)\}d\Omega \\ &\quad +\gamma\int_{\Omega}\frac{\partial\delta q_3}{\partial x_3}\left(\frac{\partial q_1}{\partial x_1} + \frac{\partial q_2}{\partial x_2} + \frac{\partial q_3}{\partial x_3}\right)d\Omega \\ &\quad -\int_{\Omega}\rho\delta q_3\bar{b}_3 d\Omega - \oint_{\Gamma}\delta q_3 t_3 d\Gamma \end{aligned} \tag{21}$$

In the equations (19) through (21), the continuity condition is included through the constraint equation. It is therefore possible to compare these equations with the weak form of the momentum equation (6) and to set up the following relationship between pressure and the constraint equation:

$$-\in\bar{p} = \gamma\int_{\Omega} G d\Omega = \gamma\int_{\Omega}(q_{\mathrm{j,j}})\,d\Omega \tag{22}$$

Finite element equations

The finite element approach employed here will be based on an assumed discharge velocity field in each finite element. Since the functional $\mathcal{F}$ contains only first order spatial derivatives of the unknown field, convergence of the numerical solution is guaranteed if at least the zero order derivative of the discharge velocity is taken as nodal unknowns and if the spatial interpolation field is a complete polynomial of at least degree one. The assumed specific discharge field can therefore be expressed as

$$q_{\mathrm{i}} = \sum_{\beta=1}^{m}\psi_\beta(x, y, z)\,q_{\mathrm{i}\beta} \tag{23}$$

where the ψ_β are interpolation functions, $q_{\mathrm{i}\beta}$ are the i-component of the unknown nodal values of the specific discharge and m is the number of nodes per element.

According to the method of Ritz the m equations needed to solve for the m nodal unknowns per element are generated by setting $\delta q_1 = \psi_\alpha$ for $\alpha = 1$ to m. The set of algebraic equations generated per element in this way can be ordered and summarized in the following matrix format:

$$\begin{bmatrix} K^{11}_{\alpha\beta} & K^{12}_{\alpha\beta} & K^{13}_{\alpha\beta} \\ K^{21}_{\alpha\beta} & K^{22}_{\alpha\beta} & K^{23}_{\alpha\beta} \\ K^{31}_{\alpha\beta} & K^{32}_{\alpha\beta} & K^{33}_{\alpha\beta} \end{bmatrix}\begin{Bmatrix} q_{1\beta} \\ q_{2\beta} \\ q_{3\beta} \end{Bmatrix} = \begin{Bmatrix} F^1_\alpha \\ F^2_\alpha \\ F^3_\alpha \end{Bmatrix} \tag{24}$$
$$\alpha, \beta = 1, 2 \ldots m$$

where

$$K^{11}_{\alpha\beta} = \int_\Omega \{2\mu \frac{\partial\psi_\alpha}{\partial x_1}\frac{\partial\psi_\beta}{\partial x_1} + \mu \frac{\partial\psi_\alpha}{\partial x_2}\frac{\partial\psi_\beta}{\partial x_2} + \mu \frac{\partial\psi_\alpha}{\partial x_3}\frac{\partial\psi_\beta}{\partial x_3} + \mu F_{11}\psi_\alpha\psi_\beta\} d\Omega + \gamma \int_\Omega \frac{\partial\psi_\alpha}{\partial x_1}\frac{\partial\psi_\beta}{\partial x_1} d\Omega \quad (25)$$

$$K^{12}_{\alpha\beta} = \int_\Omega \left\{\mu \frac{\partial\psi_\alpha}{\partial x_2}\frac{\partial\psi_\beta}{\partial x_1} + \mu F_{12}\psi_\alpha\psi_\beta\right\} d\Omega + \gamma \int_\Omega \frac{\partial\psi_\alpha}{\partial x_1}\frac{\partial\psi_\beta}{\partial x_2} d\Omega \quad (26)$$

$$K^{13}_{\alpha\beta} = \int_\Omega \left\{\mu \frac{\partial\psi_\alpha}{\partial x_3}\frac{\partial\psi_\beta}{\partial x_1} + \mu F_{13}\psi_\alpha\psi_\beta\right\} d\Omega + \gamma \int_\Omega \frac{\partial\psi_\alpha}{\partial x_1}\frac{\partial\psi_\beta}{\partial x_3} d\Omega \quad (27)$$

$$K^{21}_{\alpha\beta} = \int_\Omega \left\{\mu \frac{\partial\psi_\alpha}{\partial x_1}\frac{\partial\psi_\beta}{\partial x_2} + \mu F_{21}\psi_\alpha\psi_\beta\right\} d\Omega + \gamma \int_\Omega \frac{\partial\psi_\alpha}{\partial x_2}\frac{\partial\psi_\beta}{\partial x_1} d\Omega \quad (28)$$

$$K^{22}_{\alpha\beta} = \int_\Omega \{2\mu \frac{\partial\psi_\alpha}{\partial x_2}\frac{\partial\psi_\beta}{\partial x_2} + \mu \frac{\partial\psi_\alpha}{\partial x_1}\frac{\partial\psi_\beta}{\partial x_1} + \mu \frac{\partial\psi_\alpha}{\partial x_3}\frac{\partial\psi_\beta}{\partial x_3} + \mu F_{22}\psi_\alpha\psi_\beta\} d\Omega + \gamma \int_\Omega \frac{\partial\psi_\alpha}{\partial x_2}\frac{\partial\psi_\beta}{\partial x_2} d\Omega \quad (29)$$

$$K^{23}_{\alpha\beta} = \int_\Omega \left\{\mu \frac{\partial\psi_\alpha}{\partial x_3}\frac{\partial\psi_\beta}{\partial x_2} + \mu F_{23}\psi_\alpha\psi_\beta\right\} d\Omega + \gamma \int_\Omega \frac{\partial\psi_\alpha}{\partial x_2}\frac{\partial\psi_\beta}{\partial x_3} d\Omega \quad (30)$$

$$K^{31}_{\alpha\beta} = \int_\Omega \left\{\mu \frac{\partial\psi_\alpha}{\partial x_1}\frac{\partial\psi_\beta}{\partial x_3} + \mu F_{31}\psi_\alpha\psi_\beta\right\} d\Omega + \gamma \int_\Omega \frac{\partial\psi_\alpha}{\partial x_3}\frac{\partial\psi_\beta}{\partial x_1} d\Omega \quad (31)$$

$$K^{32}_{\alpha\beta} = \int_\Omega \left\{\mu \frac{\partial\psi_\alpha}{\partial x_2}\frac{\partial\psi_\beta}{\partial x_3} + \mu F_{32}\psi_\alpha\psi_\beta\right\} d\Omega + \gamma \int_\Omega \frac{\partial\psi_\alpha}{\partial x_3}\frac{\partial\psi_\beta}{\partial x_2} d\Omega \quad (32)$$

$$K^{33}_{\alpha\beta} = \int_\Omega \{2\mu \frac{\partial\psi_\alpha}{\partial x_3}\frac{\partial\psi_\beta}{\partial x_3} + \mu \frac{\partial\psi_\alpha}{\partial x_1}\frac{\partial\psi_\beta}{\partial x_1} + \mu \frac{\partial\psi_\alpha}{\partial x_2}\frac{\partial\psi_\beta}{\partial x_2} + \mu F_{33}\psi_\alpha\psi_\beta\} d\Omega + \gamma \int_\Omega \frac{\partial\psi_\alpha}{\partial x_3}\frac{\partial\psi_\beta}{\partial x_3} d\Omega \quad (33)$$

$$F^1_\alpha = \int_\Omega \psi_\alpha \rho b_1 d\Omega + \oint_\Gamma \psi_\alpha t_{1d\Gamma} \quad (34)$$

$$F^2_\alpha = \int_\Omega \psi_\alpha \rho b_2 d\Omega + \oint_\Gamma \psi_\alpha t_{2d\Gamma} \quad (35)$$

and

$$F^3_\alpha = \int_\Omega \psi_\alpha \rho b_3 d\Omega + \oint_\Gamma \psi_\alpha t_{3d\Gamma} \quad (36)$$

Computer implementation

Software development

The finite element equations (25) through (36) are very similar in form and nature to the governing equations for laminar flows of viscous incompressible fluids and the computer implementation therefore relies to a large extent on numerical experience gained and reported in the literature on finite element analyses of this type of problem. In this context the following specific conclusions and recommendations listed by Reddy[8] were incorporated in the developed software:

- Reduced integration is used for all terms in the stiffness matrix associated with the penalty parameter, i.e. these terms are numerically integrated using an integration order rule of one order less than that required to integrate the terms exactly. This prevents 'locking' of the numerical solution by the penalty function as the value of the penalty parameter is increased and therefore allows greater freedom with respect to the selection of the penalty parameter.
- Computation of pressures at the full integration points is less accurate than pressures computed at the reduced integration points. Pressure results are therefore computed at reduced integration points.

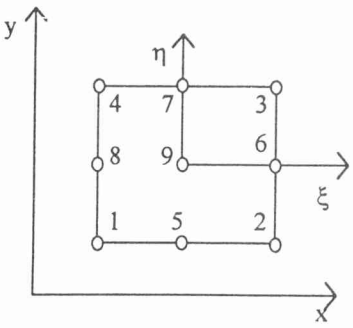

$\psi_1 = (\xi^2 - \xi)(\eta^2 - \eta)/4$
$\psi_2 = (\xi^2 + \xi)(\eta^2 - \eta)/4$
$\psi_3 = (\xi^2 + \xi)(\eta^2 + \eta)/4$
$\psi_4 = (\xi^2 - \xi)(\eta^2 + \eta)/4$
$\psi_5 = (1 - \xi^2)(\eta^2 - \eta)/2$
$\psi_6 = (\xi^2 + \xi)(1 - \eta^2)/2$
$\psi_7 = (1 - \xi^2)(\eta^2 + \eta)/2$
$\psi_8 = (\xi^2 - \xi)(1 - \eta^2)/2$
$\psi_9 = (1 - \xi^2)(1 - \eta^2)$

Figure 1 The 9-node Lagrangian isoparametric finite element and associated shape functions

- Quadratic rectangular elements yield more reliable pressure results than linear rectangular or linear/quadratic triangular elements. All results listed will therefore be for 9-node Lagrangian isoparametric elements as shown in Figure 1. See Reddy[8]

and/or Cook *et al.*[9] for a detailed description of this element as well as the isoparametric formulation concept.

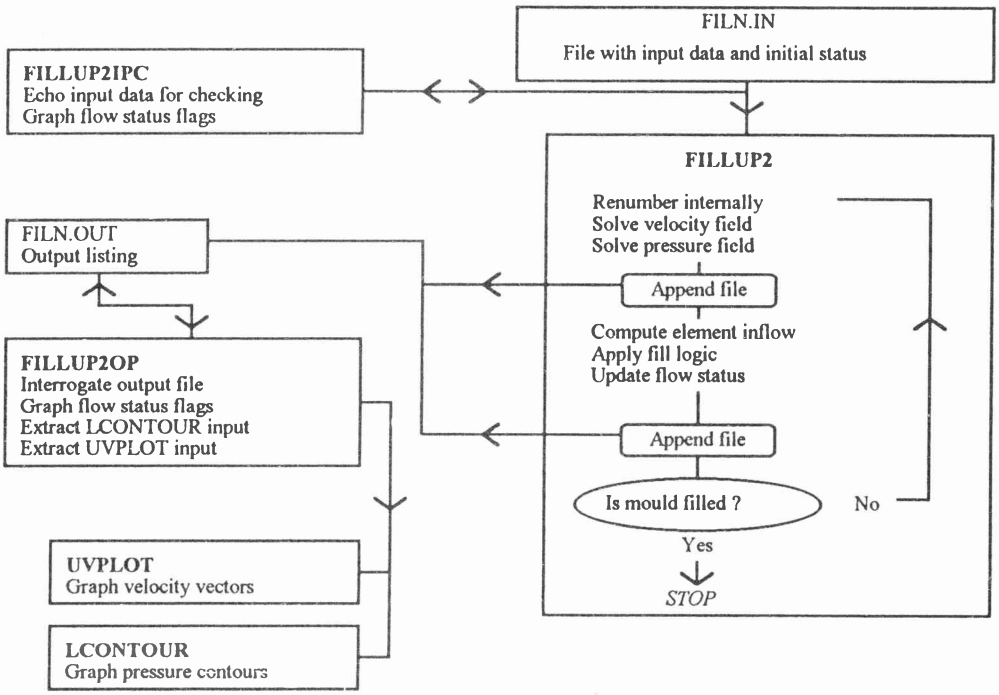

Figure 2 Functional diagram of FILLUP2 and auxiliary software

A computer program FILLUP2 was written to solve two-dimensional macroscopic flow through porous media. Auxiliary software was generated to function with the program to enable input data generation, input data checking and the interrogation of output results. A functional diagram of the main and auxiliary programs are given in Figure 2.

The program was also set up as part of a logic procedure to simulate the penetration of a liquid phase into a porous domain filled initially with a gaseous substance under the assumptions of negligible gas pressure and a rigid porous domain. The underlying approach of the latter procedure is to generate the finite element mesh of the complete porous domain as an input file. Those elements and nodes that represent areas of the domain, that are saturated with fluid at each time step, are identified through a set of status flags. This 'active' part of the problem is then solved numerically for velocities and pressures. The fluid velocity on the free surface of the fluid is evaluated to determine whether those 'inactive' elements adjacent to the free surface will fill up and become 'active' for the next time step. Based on this evaluation the model status flags are reset to redefine the 'active' part of the domain and the analysis can be repeated for the next time step. Extraction of the 'active' part of the problem from the input file at each time step, as well the status flag settings, are done automatically by the software.

Software verification – Case Study 1

Table 1 compares the results from FILLUP2 with an approximate analytical solution presented by Nadai[10] for the flow of a viscous incompressible material squeezed between two long parallel plates. To do this type of analysis with FILLUP2 the flow resistance F_{ij} must be set to zero and the porosity of the porous medium must be set to one. The finite element boundary conditions as well as the mesh are shown in Figure 3.

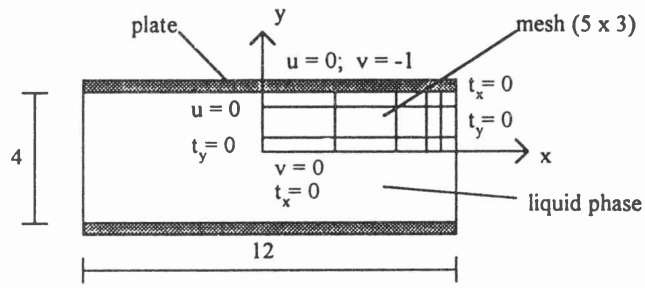

Figure 3 Finite element mesh for comparison with the Nadai[10] solution

Table 1 Comparison of FILLUP2 u-velocity results with the Nadai[10] solution

x-coordinate	FILLUP2 $\gamma=1$ $\mu=1$	FILLUP2 $\gamma=100$ $\mu=1$	FILLUP2 $\gamma=10^8$ $\mu=1$	Nadia solution[10]
1.0	0.0310	0.6513	0.7505	0.7500
2.0	0.0691	1.3062	1.4992	1.5000
3.0	0.1233	1.9769	2.2557	2.2500
4.0	0.2061	2.6730	3.0238	3.0000
4.5	0.2631	3.0463	3.4307	3.3750
5.0	0.3310	3.3956	3.8029	3.7500
5.25	0.3684	3.5732	3.9944	3.9375
5.5	0.4064	3.6874	4.1058	4.1250
5.75	0.4443	3.7924	4.2160	4.3125
6.0	0.4797	3.7862	4.1937	4.5000

Software verification – Case Study 2

Figures 4 and 5 show results for two-dimensional developing flow between two flat plates with varying flow resistance to viscosity ratios. The figures show how the velocity and pressure distributions change with increasing flow resistance of the porous domain, until the solution converges to the one-dimensional Darcy-type flow at a flow resistance to viscosity ratio of 1 000. The 4.0 × 2.0 cross-sectional area is meshed with 6×4 9-node elements and the boundary conditions consisted of a uniform unit inlet velocity and no-slip along the horizontal edges. (Note that the relationship between permeability and shear flow resistance was established by Du Plessis & Masliyah[6] as $\in = FK$.)

Liquid penetration simulation

This section is included to illustrate the use of the software to simulate the penetration of a liquid phase into the voids of an 'empty' porous domain. Figure 6 shows the finite element mesh used to model the 0.3 m × 0.1 m cross-section of a long porous domain. The liquid viscosity was taken as 0.5 Ns/m^2, together with an assumed orthotropic flow resistance of 10 000 m^{-2} in the horizontal direction and 1 000 m^{-2}, in the vertical direction.

The porosity was taken as constant = 0.5 throughout the domain. Gravity forces are ignored and the penalty parameter was selected at 1.0E08. Initially one element (number 81) is saturated with the liquid phase. Boundary conditions consist of no-slip along the edges of the domain with an applied discharge of 0.001 m/s over the outer edge of element 81. Figure 7 shows the saturation state of the domain at the indicated times. Elements that are completely filled with the liquid phase are hatched with a cross. The total time predicted by FILLUP2 to fill the porous domain is 1 016 seconds. This

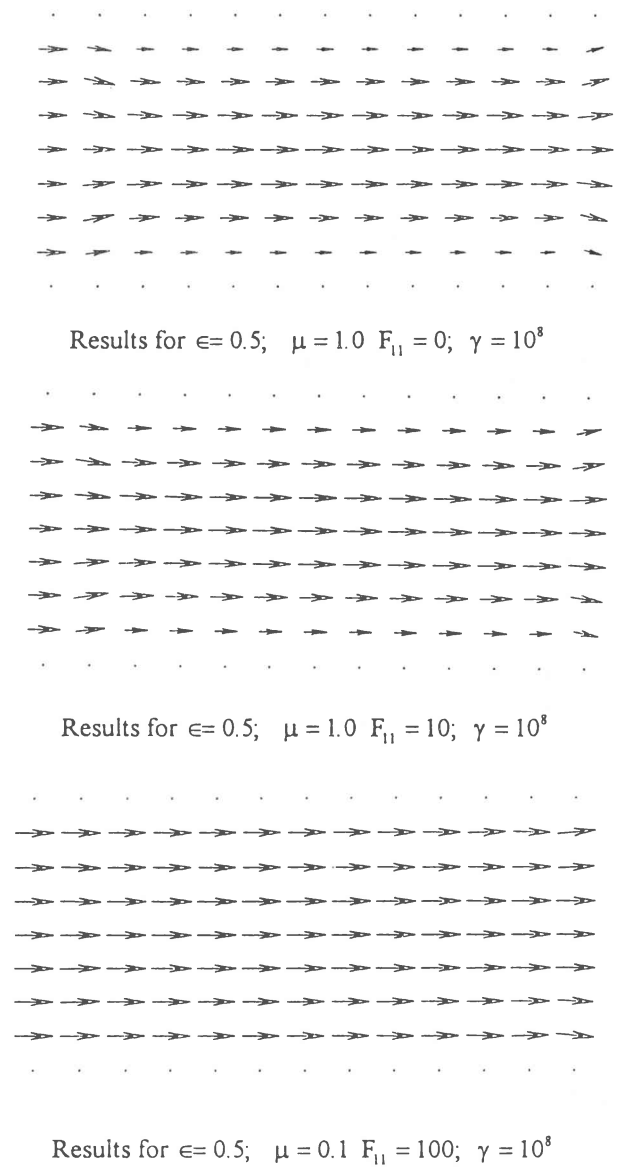

Figure 4 Developing flow analysis – velocity vectors

value compares well with the exact value calculated from global continuity of 1 009 seconds.

Discussion

Equations (24) through (36) and the numerical results summarized in Figures 4, 5, and 7 illustrate the relative ease with which the phase average Navier-Stokes equation can be solved with the finite element method using the penalty function technique to ensure continuity. The various terms in the stiffness matrix, as well as the natural boundary conditions have physical appeal and are easy to implement.

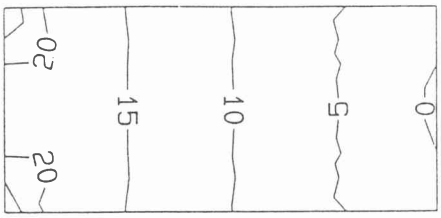

Results for $\epsilon = 0.5$; $\mu = 1.0$ $F_{11} = 0$; $\gamma = 10^8$

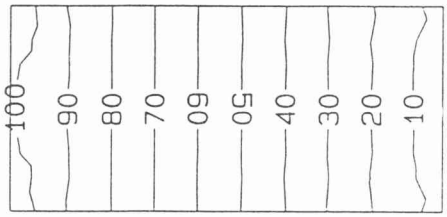

Results for $\epsilon = 0.5$; $\mu = 1.0$ $F_{11} = 10$; $\gamma = 10^8$

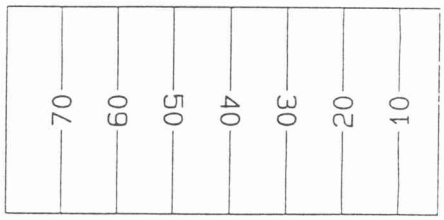

Results for $\epsilon = 0.5$; $\mu = 0.1$ $F_{11} = 100$; $\gamma = 10^8$

Figure 5 Developing flow analysis — pressure contours

161	162	163	164	165	166	167	168	169	170	171	172	173	174	175	176	177	178	179	180
141	142	143	144	145	146	147	148	149	150	151	152	153	154	155	156	157	158	159	160
121	122	123	124	125	126	127	128	129	130	131	132	133	134	135	136	137	138	139	140
101	102	103	104	105	106	107	108	109	110	111	112	113	114	115	116	117	118	119	120
81	82	83	84	85	86	87	88	89	90	91	92	93	94	95	96	97	98	99	100
61	62	63	64	65	66	67	68	69	70	71	72	73	74	75	76	77	78	79	80
41	42	43	44	45	46	47	48	49	50	51	52	53	54	55	56	57	58	59	60
21	22	23	24	25	26	27	28	29	30	31	32	33	34	35	36	37	38	39	40
1	2	3	4	5	6	7	8	9	10	11	12	13	14	15	16	17	18	19	20

Figure 6 Finite element model for Liquid Penetration Simulation (status at time = 0 seconds)

It can be seen from equation (17) that the extent to which the continuity constraint will be satisfied will depend on the relative magnitude of the penalty parameter γ. For a very large value of γ the constraint will dominate the solution and make the solution insensitive to the governing equations. For a small value of γ the participation of the constraint equation in the solution vanishes. Reddy[8] recommends a penalty parameter to viscosity ratio of 10^4 to 10^{12} for good results during the analysis of laminar flows of viscous incompressible fluids. For the present type of analysis, results were found to be satisfactory if both the penalty parameter to viscosity ratio and the penalty parameter to shear flow resistance ratio were kept within the 10^4 to 10^{12} bounds.

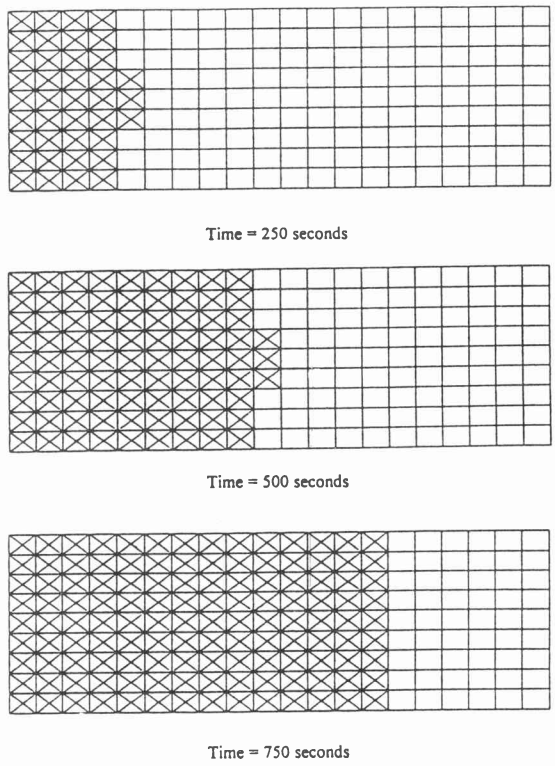

Figure 7 Porous domain fill status at selected times

In some practical problems the situation may however arise where the physical shear flow resistance to viscosity ratios are too large to select a penalty parameter according to the above guidelines. In situations like this the physical implication is that macroscopic boundary effects no longer play a significant role in the solution and the Darcy equation (1) should be used instead of the phase average Navier-Stokes equation (3) to govern equilibrium. It is of course quite possible to still use the presented solution method with a false (larger) viscosity and to obtain accurate results, but this would be counterproductive since the finite element solution of the Darcy equation is much simpler in form than that of the phase average Navier-Stokes equation and since several commercial finite element codes can handle the Darcy-type problem in a very powerful way.

Conclusion

The finite element algebraic equations are presented for the phase average Navier- Stokes equation and the continuity equation governing transport in porous media.

The presented equations are for low Reynolds number steady state flow of viscous incompressible fluids. Numerical results are included to illustrate the correctness and ease of implementation of the algebraic equations. The latter is emphasized by the simplistic, yet useful, control volume flow logic of FILLUP2 for the modelling of fluid penetration into 'dry' porous domains.

The extension of the present results to unsteady flow, as well as the 3-dimensional numerical implementation of the presented equations, is a straightforward exercise and further illustrates the usefulness of the form of the phase average Navier-Stokes equation presented by Du Plessis & Masliyah[6] as tool for numerical finite element analysis of seepage problems.

REFERENCES

[1] Darcy HPG, Les Fontaines Publiques de la Ville de Dijon, Victor Dalmont, Paris, 1856, *cf.* Muskat M. *The Flow of Homogeneous Fluids through Porous Media.* McGraw-Hill, New York, 1937.

[2] Bruschke MV & Advani SG. A Finite Element/Control Volume Approach to Mold Filling in Anisotropic Porous Media. *Polymer Composites*, **11**, 1990, 398–405.

[3] Slattery JC. Single Phase Flow through Porous Media. *Am. Inst. Chem. Eng. J.*, **15**, 1969, 886–872.

[4] Whitaker S. Diffusion and Dispersion in Porous Media. *Am. Inst. Chem. Eng. J.*, **13**, 1967, 420–427.

[5] Bear J & Bachmat Y. Macroscopic Modelling of Transport Phenomena in Porous Media 2: Application to Mass, Momentum and Energy Transport. *Transport in Porous Media*, **1**, 1986, 241–269.

[6] Du Plessis JP & Masliyah JH. Mathematical Modelling of Flow through Consolidated Isotropic Porous Media. *Transport in Porous Media*, **3**, 1988, 145–161.

[7] Van der Westhuizen J & Du Plessis JP. Quantification of Unidirectional Fiber Bed Permeability. *J. of Comp. Materials*, **7**, 1994, 619.

[8] Reddy JN. *An Introduction to the Finite Element Method,* 2nd edn. McGraw-Hill, 1993.

[9] Cook RD, Malkus DS & Plesha ME. *Concepts and Applications of Finite Element Analysis*, 3rd edn. J. Wiley, 1989.

[10] Nadai A. *Theory of Flow and Fracture of Solids*, **II**, McGraw-Hill, 1963.